


Cite this: *Mater. Adv.*, 2022,
3, 8168

Low ice adhesion anti-icing coatings based on PEG release from mesoporous silica particle loaded SBS†

Aatif Ijaz, Annamaria Miko and A. Levent Demirel *

Release-based extremely low ice adhesion strength and durable anti-icing coatings were designed and realized by loading mesoporous silica particles (MSP) into the SBS polymer matrix and filling poly(ethylene glycol) (PEG) as the anti-icing agent into MSP/SBS composites. This approach allows the formation of a thin lubricating liquid layer of PEG and water at the ice/composite interface at sub-zero temperatures and results in ice adhesion strength as low as 3 kPa. The high specific surface area of MSP ($428 \text{ m}^2 \text{ g}^{-1}$) as the anti-icing agent carrier significantly contributed to the retainment of PEG in the composites. The freezing time of water droplets on the composites increased and the ice adhesion strength decreased with the amount of PEG retained in the composites. After 15 icing/deicing cycles, the ice adhesion strength was measured to be ~ 5 kPa indicating a rather slow release (and removal with ice) of PEG at -10 °C from surface-exposed pores of MSP. The importance of PEG at the ice/composite interface was confirmed by ice adhesion strength measurements of frozen PEG-containing aqueous solutions on unfilled MSP/SBS composites. These results clearly show that PEG filled MSP/SBS composites demonstrate a passive anti-icing mechanism based on sustained release of PEG with extremely low ice adhesion strength and significant potential for longer-term use in sub-zero temperature and harsh environments.

Received 9th June 2022,
Accepted 20th August 2022

DOI: 10.1039/d2ma00661h

rsc.li/materials-advances

Introduction

Ice accumulation on surfaces significantly affects safe and smooth daily operations and causes severe problems such as accidents, power outages and structural damage.¹ Passive anti-icing coatings have been considered as an easy, economical and eco-friendly approach to overcome the icing problems due to their ability to suppress ice formation and accumulation without any energy input, but their widespread use in applications still remains a challenge.^{2–6} Icephobic coatings can delay ice formation,^{7–9} lower ice adhesion strength^{4,6,10} and allow easy removal of accumulated ice¹¹ by various mechanisms such as superhydrophobicity,^{5,8,12–14} sacrificial lubricants,^{6,15} interfacial slippage^{16,17} and release.^{18,19} Typically, the ice adhesion strength on these coatings is lower than 100 kPa. The ice adhesion strength was estimated to be lower than 12 kPa for the accumulated ice to easily shed off under the action of wind or gravity.¹⁷

Superhydrophobic surfaces with hierarchical micro/nano-sized roughness on low surface energy components, a water contact angle larger than 150° and a low wetting hysteresis have been extensively used to delay ice nucleation and prevent ice accumulation.^{5,12,14} High contact angles, low sliding angles and the air entrapped underneath the water droplets on micro/nano-sized rough superhydrophobic surfaces have contributed to icephobicity through different mechanisms involving easy removal of liquid droplets on the surfaces, delay in crystallization of water droplets, decreased heat transfer between the droplet and the surface, decrease in adhesion of ice and snow to the surface and as a result decrease in ice, snow, and frost accumulation on surfaces. However, superhydrophobic surfaces display mechanical weakness and increased ice adhesion strength at sub-zero temperatures due to ice nucleation within their hierarchical surface structures, preferably on the wetting defects.^{20–22} Micro- and nanotexturing of the surface layer of aluminium together with chemical modification was reported to enhance wear and chemical resistance of the surfaces and overcome the main drawbacks of superhydrophobic icephobic coatings.²²

Slippery liquid-infused porous surfaces (SLIPS) have also been widely used to overcome the vulnerability of superhydrophobic surfaces.²³ The mobile lubricant layer, typically

Chemistry Department, Koç University, 34450, Sarıyer, Istanbul, Turkey.
E-mail: ldemirel@ku.edu.tr

† Electronic supplementary information (ESI) available: SEM, EDX, and TGA of filled MSP; ice adhesion strength and frost accumulation data of composites. See DOI: <https://doi.org/10.1039/d2ma00661h>



low-surface-tension liquids, of SLIPS prevents the pinning of the contact line that results in low sliding angles and decreases the ice adhesion strength down to ~ 10 kPa.^{6,15} The grafting of polydimethylsiloxane chains on substrates resulted in a low ice adhesion strength of ~ 15 kPa while preventing the depletion of the mobile layer and the increase in ice adhesion strength in time.²⁴ Different approaches were used to enhance SLIPS durability.^{25–27} Hydrophilic lubricating liquids filled in hydrophilic porous surfaces were also reported to decrease both ice accumulation and ice adhesion strength at sub-zero temperatures.²⁸ However, the removal of water-soluble hydrophilic lubricants from the support is expected to be even faster compared to that of hydrophobic lubricants due to rain or snow.

The use of hydrophilic components in anti-icing strategies introduces a self-lubricating water layer between ice and substrate which significantly contributes to the reduction of the ice adhesion strength down to ~ 20 – 30 kPa.^{29–33} This approach has mostly been limited to grafted and/or cross-linked systems to prevent the removal of the hydrophilic components. When micropores fabricated on silicon wafers were grafted with cross-linked hygroscopic polymer poly-acrylic acid, an ice adhesion strength of 55 ± 15 kPa was obtained.³⁰ Blending of PDMS-PEG copolymers in the PDMS elastomer resulted in an ice adhesion strength of $\sim 50 \pm 9$ kPa.³¹ This was attributed to the presence of nonfrozen water which served as a viscous self-lubricating interfacial layer as confirmed by solid state NMR down to -20 °C. The hydrogen bonds between PEG segregated to the ice/coating interface and the water molecules prevented freezing at the interface.³¹ Superhydrophilic polyelectrolyte brushes coated on glass were found to reduce ice adhesion by ~ 60 to 80% at -10 °C relative to bare glass. This was attributed to the enhancement of the quasi liquid layer at the interface in the presence of highly hydrated ions.³² In the same study, PEG brushes decreased ice adhesion by $\sim 55\%$ at -10 °C relative to bare glass. When polyurethane particles with hydrophilic pendant groups were spin coated on various substrates, the ice adhesion strength was observed to decrease with the weight% of the hydrophilic component down to ~ 30 kPa at -15 °C.³³

Rather few strategies based on the release of hydrophilic anti-icing agents from solid surfaces to prevent icing were reported. Ionic salts and glycols were typically used as anti-icing agents in release based approaches. The release of KCOOH stabilized by nanoparticles and gelation in an SBS matrix was reported to delay freezing of water droplets on the composite surface³⁴ and on modified bitumen.³⁵ One practical reason for the limited use of release-based systems is that their lifetime is limited by the duration of release. When the release of the active agents from the coating stops, then the coating needs to be reconstructed completely for the functionality of the surface to be continued. Slowing down the release of the anti-icing agents is a way of achieving longer-term durability of the anti-icing properties. Titanium alkoxide-based sol-gel anti-icing coatings were reported to facilitate the slow release of tripropylene glycol (TPG) and glycerol.³⁶ Surface icing responsive anti-icing agent release was reported by combining an

inner anti-icing agent filled hydrophilic membrane with an outer superhydrophobic porous layer.³⁷ We have previously reported Diatomaceous Earth (DE) loaded Styrene-Butadiene-Styrene (SBS) based composites as polyethylene glycol (PEG) releasing anti-icing coatings which delayed the freezing of water droplets.¹⁸ DE was used as a PEG carrier in the hydrophobic SBS matrix. Anti-icing agents were filled into DE pores using a novel method in which the SBS matrix was swollen to allow the diffusion of the anti-icing agents into the pores. This method also allows consecutive refilling of DE pores with PEG after the complete release of the active agents. The possibility of refilling significantly improves the lifetime of the release-based anti-icing coatings.³⁸ PEG is an effective anti-ice nucleating agent.^{39,40} An ice adhesion strength of 15 – 30 kPa was measured with PEG-400 ($M_w = 400$ g mol⁻¹) as the anti-icing agent in a microporous silica containing cross-linked PDMS matrix.¹⁹ Ethylene Glycol (EG) infused poly(ethylene imine)/silica nanoparticle layer-by-layer films exhibited an ice adhesion strength of ~ 15 kPa at -10 °C.⁴¹

With the anticipation that hydrophilic anti-icing agents released from solid surfaces into water should act better in forming a self-lubricating water layer between ice and substrate and in enhancing the icephobicity, the major motivation for this work has been to increase the amount of the anti-icing agent loaded into the polymer composite and to slow down its release by utilizing mesoporous silica particles (MSP) as an anti-icing agent carrier in the SBS matrix. MSP have the advantage of high loading capacity, chemical stability and easy surface functionalization. The non-toxic nature, large specific surface area, tunable shape, pore size and volume make MSP suitable for adsorption and release of active agents in applications ranging from drug and gene delivery to the removal of hazardous pesticides from the environment.⁴²

In this work, we have investigated the anti-icing properties of the release-based icephobic coatings realized by loading MSP into the SBS polymer matrix and filling poly(ethylene glycol) (PEG) as the anti-icing agent into MSP/SBS composites. The high specific surface area of MSP resulted in enhanced loading of the anti-icing agents into the polymer matrix while smaller pore sizes contributed to the controlled release of anti-icing agents. The coatings demonstrated extremely low ice adhesion strength which was attributed to the formation of a self-lubricating liquid layer of PEG and water due to the release of the anti-icing agent at the ice/composite interface. MSP/SBS composite coatings maintained their low ice adhesion strength for consecutive icing/de-icing cycles.

Experimental section

Materials

The Styrene-Butadiene-Styrene (SBS) (Kraton D1101 AU) linear triblock copolymer containing 31% by weight styrene content was kindly supplied by Kraton and used as the polymer matrix. Tetraethylorthosilicate (TEOS), Pluronic F127 [(poly(ethylene oxide)₁₀₆-poly(propylene oxide)₇₀-poly(ethylene oxide)₁₀₆] and



hydrochloric acid (HCl) were purchased from Sigma Aldrich and used as the silica precursor, surfactant and catalyst, respectively, in the synthesis of mesoporous silica particles (MSP). Polyethylene glycol (PEG-600, $M_w = 600 \text{ g mol}^{-1}$ and PEG-10k, $M_w = 10\,000 \text{ g mol}^{-1}$) was purchased from Merck and used as the anti-icing agent. Acetone, diethyl ether and chloroform were purchased from Merck. Bismuth subnitrate (BiONO_3) and potassium iodide (KI) used for UV-vis characterization of PEG were purchased from Sigma Aldrich. All chemicals were used without any further purification process.

Synthesis and characterization of MSP

MSP were synthesized by a block copolymer templating method as reported earlier.⁴³ The synthesis was achieved in aqueous solutions at room temperature using Pluronic F127 as the surfactant, TEOS as the precursor and HCl as the catalyst. 10 mg mL^{-1} Pluronic F127 was dissolved in the aqueous solution of 7 M HCl. 200 μL of TEOS was added at once into this solution, and the sample was shaken vigorously until a white precipitate was observed. The sample was immediately cast on a Teflon plate to evaporate the solvent (water) and the reaction byproduct (ethanol) under ambient conditions for 24 h. The dried sample was calcined to remove the organic templating agent at 450 °C for 8 h. The morphology of the resulting silica was characterized by using a field-emission scanning electron microscope (FE-SEM, Zeiss Ultra Plus). A secondary electron detector was used to collect SEM images at 3–10 kV. Energy dispersive X-ray analysis (EDX) measurements were performed by using a Bruker XFlash 5010 EDX detector with 123 eV resolution. Fourier Transform Infrared Spectroscopy (FTIR, Nicolet iS50, Thermo Scientific) analysis of bare MSP and PEG filled MSP was performed in the wavenumber range of 650–4000 cm^{-1} with a resolution of 4 cm^{-1} and a collection of 64 scans. The specific surface area (SSA) of the MSP was determined by nitrogen adsorption measurements (Micromeritics ASAP 2020 HD) according to the Brunauer-Emmett-Teller (BET) isotherm.

Evaluation of PEG uptake of MSP

The ability of MSP to take PEG as the anti-icing agent into the pores was determined by filling the pores in an aqueous solution of PEG-10k. 0.2 g of MSP was placed in 10 mL of 0.1–0.3 g mL^{-1} PEG-10k aqueous solutions. The dispersions were mixed at 400 rpm for 24 h to reach a steady state. The dispersions were then centrifuged. The sediments were redispersed in deionized (DI) water and centrifuged immediately to remove PEG chains loosely bound to MSP surfaces. The amount of PEG-10k filled into the pores of MSP was determined by thermogravimetric analysis (TGA, Q500 TA Instruments). The samples were heated up to 700 °C at 10 °C min^{-1} under a constant airflow of 40 mL min^{-1} . The release of PEG-10k from MSP into the water was measured by UV-vis spectroscopy using the modified Dragendorff method.¹⁸ The concentration of PEG-10k released into 50 mL of water from 0.2 g filled MSP was determined as a function of time.

Preparation of PEG filled MSP/SBS composites

SBS composites consisting of PEG-filled MSP were prepared by first loading MSP into the SBS matrix and then filling the MSP by keeping the composite in PEG solutions of different concentrations in an acetone/diethyl ether (70/30 by volume) binary solvent mixture. SBS stock solution was prepared by dissolving 100 mg of SBS in 1 mL of chloroform. MSP were dispersed in SBS stock solution at different MSP/SBS weight ratios (0–30 weight% of MSP in the final MSP/SBS composite). The dispersions were homogenized at 900 rpm for 6 h. Free-standing composite films ($\sim 0.2 \text{ mm}$ thick) were prepared by solvent casting 7.2 mL of dispersion in Teflon plates ($6.0 \times 4.5 \text{ cm}^2$). The films were removed from the Teflon plates after 24 h and dried in an open atmosphere.

Free-standing MSP/SBS composites were filled with PEG (PEG-600 or PEG-10k) by dipping the composite films in PEG solution in an acetone/diethyl ether (70/30 by volume) binary solvent mixture.¹⁸ In the binary solvent mixture of acetone/diethyl ether, the SBS matrix is swollen and this allows the penetration of the dissolved PEG into the pores of MSP dispersed throughout the SBS matrix. PEG-10k (solid at room temperature) was primarily chosen to quantify the filled/released amount of PEG by UV-vis spectroscopy using the modified Dragendorff method, because the sensitivity of the method is better for higher molar masses of PEG.⁴⁴ Lower molar mass PEG-600 (fluid at room temperature) was preferred to facilitate the diffusion of PEG into the SBS matrix in anti-icing applications. The concentration of the filling solution was varied between 0.10 and 0.30 g mL^{-1} for PEG-10k and between 10 and 50% by volume (0.11–0.56 g mL^{-1}) for PEG-600. MSP/SBS composites were kept in PEG solutions in acetone/diethyl ether (70/30 by volume) for 24 h at room temperature. After 24 h, the samples were rinsed with DI water, dried in an open atmosphere and then characterized for icephobic properties.

Characterization of MSP/SBS composites

The distribution of MSP in the SBS matrix was characterized by FE-SEM (Zeiss, Ultra Plus). The optical contact angle system (Dataphysics OCA 20) was used to measure the water contact angles on the MSP/SBS composites at a relative humidity of ~ 30 –50% at room temperature. The static contact angle measurements were done between 25 °C and -10 °C by placing three water droplets of 5 μL volume on the MSP/SBS composite surface.

The freezing delay of water droplets on MSP/SBS composites as a function of temperature was also investigated in a Dataphysics OCA 20 sample cell. Composite samples were placed in the instrument cell at 25 °C and then the temperature was decreased. The measurements were performed at the cell stage temperature of -15 to -10 °C after 5 min stabilization. The delay in the freezing of 5 μL water droplets was measured by using a video camera attached to the instrument. 5 droplets were measured on each substrate and the measurement was repeated on 3 different substrates.



Frost accumulation experiments were carried out in a chamber at $-10\text{ }^{\circ}\text{C}$. The samples were attached to a metal plate and placed at an inclination angle of 45° inside the icing chamber for 30 minutes. To simulate the frost formation, water was sprayed from a precooled ice and water mixture ($0\text{ }^{\circ}\text{C}$) through a spray nozzle onto the samples from a fixed distance of 18 cm. The amount of water sprayed out of the nozzle was estimated to be 0.75 mL min^{-1} . The amount of frost accumulated on the samples was determined gravimetrically. Frost accumulation experiments were repeated 3 times.

Ice adhesion measurements

Ice adhesion measurements were performed with a force sensor using an environmentally controlled setup designed and manufactured by Teknofil Ltd, Istanbul (Fig. S1a, ESI[†]). MSP/SBS composites were solvent cast on glass slides ($2.4 \times 3.2\text{ cm}^2$) and filled with PEG in the binary solvent mixture. Ice columns ($1\text{ cm} \times 1\text{ cm} \times 4\text{ cm}$) were formed on the composite using plastic cuvettes. The samples were stabilized at the measurement temperature in the temperature-controlled chamber for 6 h. The force to detach the ice from the composite surface was measured by horizontally moving the force probe – located 2 mm above the ice/composite interface – into the side of the ice column at a constant velocity of 0.25 mm s^{-1} . The maximum force to detach the ice column (Fig. S1b, ESI[†]) was divided by the apparent cross-sectional area of the ice-composite interface to obtain the ice adhesion strength.

To investigate the effect of decreasing amount of PEG retained in the composite due to release on the ice adhesion strength, ice adhesion measurements were performed on

MSP/SBS coatings filled in 50 vol% PEG-600 aqueous solution after immersing them for a duration of 2–20 min in 10 mL of DI water and drying in open air.

The effect of the concentration of PEG on the ice adhesion strength was also checked by freezing aqueous PEG-600 and PEG-10k solutions at different concentrations ($1\text{--}20\text{ mg mL}^{-1}$) on the unfilled MSP/SBS composites as ice columns and measuring the ice adhesion strength as described above.

Results and discussion

Preparation and characterization of MSP as an anti-icing agent carrier

Composite anti-icing coatings having 0–30 weight% MSP in SBS were prepared by solvent casting and post-filling with PEG as the anti-icing agent. MSP served as the anti-icing agent carrier in the hydrophobic SBS matrix.

Micron sized spherical MSP were synthesized in acidic aqueous solution at room temperature by block copolymer templating as reported earlier.⁴³ Fig. 1a shows the SEM image of the synthesized MSP. The particles were spherical and had a diameter of $1.0 \pm 0.2\text{ }\mu\text{m}$. The nitrogen adsorption/desorption isotherm of MSP (Fig. 1b) is typical for spherical particles having a combination of mesopores (pore size of 3–4 nm) and micropores (pore size $< 2\text{ nm}$) in their structure. The specific surface area of MSP was determined by nitrogen adsorption isotherm as $428\text{ m}^2\text{ g}^{-1}$.

The potential of MSP to retain PEG as the anti-icing agent carrier was investigated. MSP were dispersed and kept in an aqueous PEG solution for 24 h. The particles were then

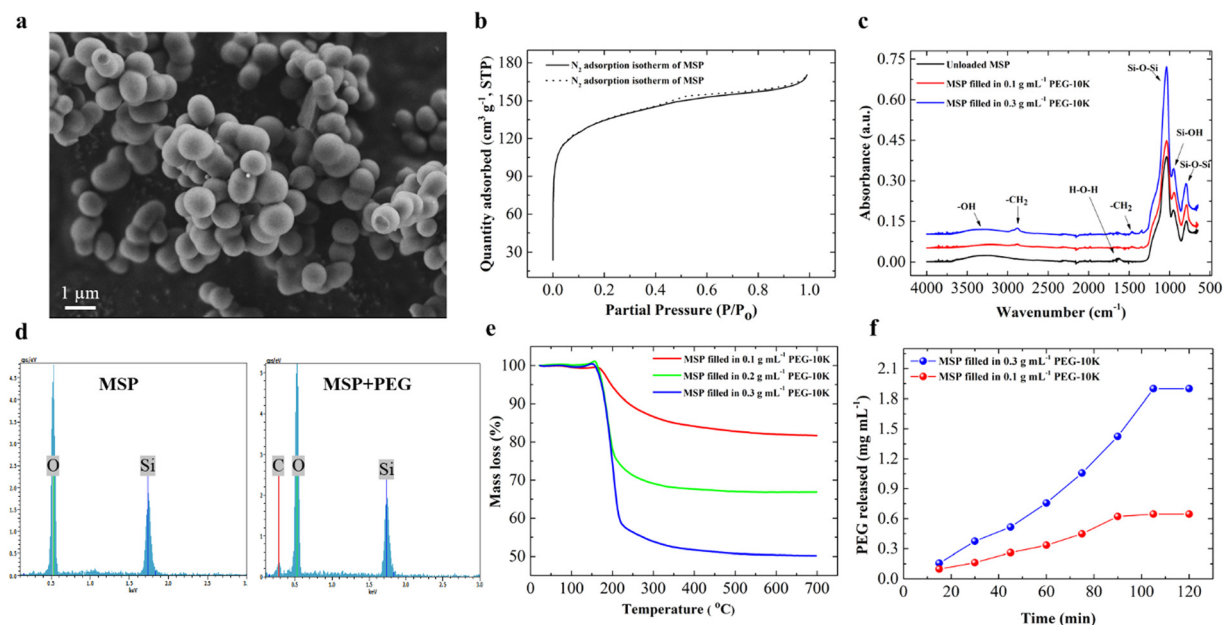


Fig. 1 Characterization of MSP and their PEG filling/releasing abilities. (a) SEM of synthesized MSP, (b) nitrogen adsorption/desorption isotherm of MSP corresponding to a specific surface area of $428\text{ m}^2\text{ g}^{-1}$, (c) FTIR spectra of bare (unfilled) MSP and MSP filled in 0.1 g mL^{-1} PEG-10k solution (red line) and MSP filled in 0.3 g mL^{-1} PEG-10k solution (blue line), (d) EDX spectra of MSP and MSP filled in 0.3 g mL^{-1} PEG-10k solution, (e) TGA of MSP filled in 0.1 g mL^{-1} (red line), 0.2 g mL^{-1} (green line) and 0.3 g mL^{-1} (blue line) PEG-10k solution, (f) Concentration of PEG-10k in time as a result of release into 50 mL of water from 0.2 g filled MSP filled in 0.1 g mL^{-1} (red spheres) and 0.3 g mL^{-1} (blue spheres) PEG-10k solution.



centrifuged, rinsed with DI water and dried in an open atmosphere. Fig. 1c shows the FTIR spectra of dried MSP kept in 0.1 g mL⁻¹ and 0.3 g mL⁻¹ PEG-10k solution (filling solutions) together with bare (unfilled) MSP. The strong vibrational bands at 1060 cm⁻¹ (asymmetric stretching) and 796 cm⁻¹ (symmetric stretching) correspond to Si–O–Si bonds. The peak at 950 cm⁻¹ is due to the bending vibrations of Si–OH groups. The overlap of stretching vibrations of –OH of physically adsorbed water and hydrogen bonds between water and Si–OH groups resulted in broad adsorption bands at 3300–3500 cm⁻¹. No –CH₂ peaks at 2894 cm⁻¹ (symmetric stretching) and 1465 cm⁻¹ (bending) are present in the IR spectrum of bare MSP, as expected. The intensity of –CH₂ bands increased with the concentration of PEG in the loading solution indicating that more PEG was filled into MSP. The observation of the C peak in EDX analysis of filled MSP (filling solution concentration of 0.3 g mL⁻¹) also confirmed the presence of PEG in MSP (Fig. 1d). A weak but significant carbon peak was observed at 0.28 keV along with oxygen (0.53 keV) and silicon (1.73 keV) peaks. Only Si and O peaks were observed in the EDX spectrum of unfilled MSP without any significant C peak. The atomic percent of carbon increased with the filling solution concentration of PEG from 5.5% at 0.1 g mL⁻¹ filling concentration to 9.5% at 0.3 g mL⁻¹ (Fig. S2, ESI[†]).

The amount of PEG filled in MSP was determined by thermogravimetric analysis (TGA). Fig. 1e shows the thermograms of MSP filled in 0.1 g mL⁻¹, 0.2 g mL⁻¹ and 0.3 g mL⁻¹ PEG-10k solution. Unfilled MSP showed a total mass loss of 4.5% due to physically adsorbed water (Fig. S3, ESI[†]). The onset of major mass loss for MSP filled with PEG-10k was observed at ~200 °C due to the decomposition of PEG (Fig. 1e). The mass% of PEG filled into MSP was determined from the thermograms as 18, 33 and 49.5 for MSP filled in 0.1 g mL⁻¹, 0.2 g mL⁻¹ and 0.3 g mL⁻¹ aqueous PEG-10k solution, respectively. Consistent with FTIR and EDX analysis, TGA clearly showed that more PEG was retained in MSP when the filling was performed in a solution of higher PEG concentration. Considering the relatively high specific surface area of MSP (428 m² g⁻¹), PEG is expected to be adsorbed inside the micro/mesopores. DE having a much smaller specific surface area of 65 m² g⁻¹ retained water soluble polymers (PEG, PEOX) in its micron sized pores.¹⁸

The relatively slow release (~2 hours) of PEG-10k from filled MSP in water also supports that PEG was retained in the pores of MSP. Fig. 1f shows the release profile of PEG-10k into water as a function of time for MSP filled in 0.1 g mL⁻¹ and 0.3 g mL⁻¹ aqueous PEG-10k solution. For both samples, the release continued for 90–100 min and then stopped. 0.160 mg (of the loaded 0.180 mg) was released after ~90 min for MSP filled in 0.1 g mL⁻¹ PEG-10k, while 0.475 mg (of the loaded 0.495 mg) was released after ~100 min for MSP filled in 0.3 g mL⁻¹ PEG-10k. For both samples, the amount of PEG that was not released was ~0.020 mg which was attributed to stronger adsorption of PEG on the surface of the MSP.

Preparation and PEG filling of anti-icing composites

After demonstrating the successful loading and release of PEG into MSP, unfilled MSP were loaded into SBS and then filled

with PEG-600 or PEG-10k for the preparation of low ice adhesion anti-icing composites.

The amount of PEG-600 retained in MSP/SBS composites after swelling mediated filling was determined gravimetrically. Fig. 2a shows the mass of PEG retained in the composites as a function of PEG-600 concentration in the binary mixture in which the composites were kept for 24 h. The amount of PEG retained in the MSP/SBS composite increased with increasing mass% of MSP in SBS. This clearly shows the role of MSP in the retention of PEG in the composites. The retained PEG is expected to be in the micro/meso pores of MSP due to favorable interfacial interactions between PEG and silica with some kinetically trapped PEG molecules in the SBS matrix. MSP/SBS composites retained approximately twice more PEG-600 as compared to DE/SBS composites (30% silica by weight in both) at the PEG-600 concentration of 50% by volume in the binary mixture (Fig. S4, ESI[†]). We attribute this to the higher specific surface area of MSP (428 m² g⁻¹) compared to DE (65 m² g⁻¹).

The amount of PEG retained also increased with increasing concentration of PEG in the binary mixture. As expected, hydrophobic SBS did not retain much PEG at any concentration. The retained amount in the composite having 30% by mass MSP increased linearly with increasing PEG concentration. When the mass% of MSP was increased above 30, the composite became brittle and could not be processed. Therefore, composites having 30% by mass MSP were used in further characterization. In 1 mg composite having 30% by mass MSP, 0.034 mg of PEG-600 was retained at 10% by volume PEG concentration, which gradually increased to 0.170 mg at 50% by volume concentration of PEG-600. Above 50 volume% of PEG, the amount of the binary mixture was not enough to swell the composite and carry the PEG chains inside the composite. Fig. 2b shows the surface morphology of MSP/SBS composites before PEG filling. No significant change was observed in the dispersion of MSP on the top surface of the SBS matrix after PEG filling as seen in Fig. 2c.

Fig. 3a and b show, respectively, the comparison of amount of PEG retained and the anti-icing efficacy of composites having 30% by mass MSP when filled with PEG-600 and PEG-10k.

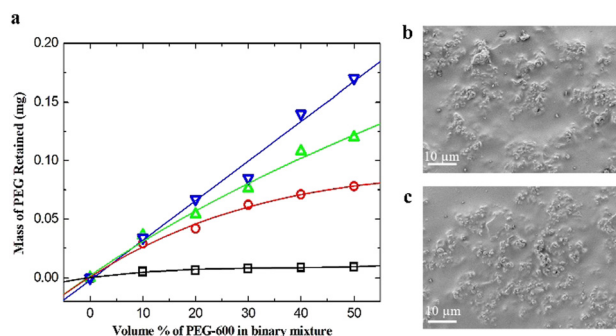


Fig. 2 (a) Mass of PEG-600 retained in 1 mg of MSP/SBS composite as a function of PEG-600 concentration in the binary solvent mixture. Mass% of MSP in SBS was 0 (squares), 10 (circles), 20 (up triangles) and 20 (down triangles). SEM image of the MSP/SBS composite (b) before PEG filling and (c) after PEG filling.



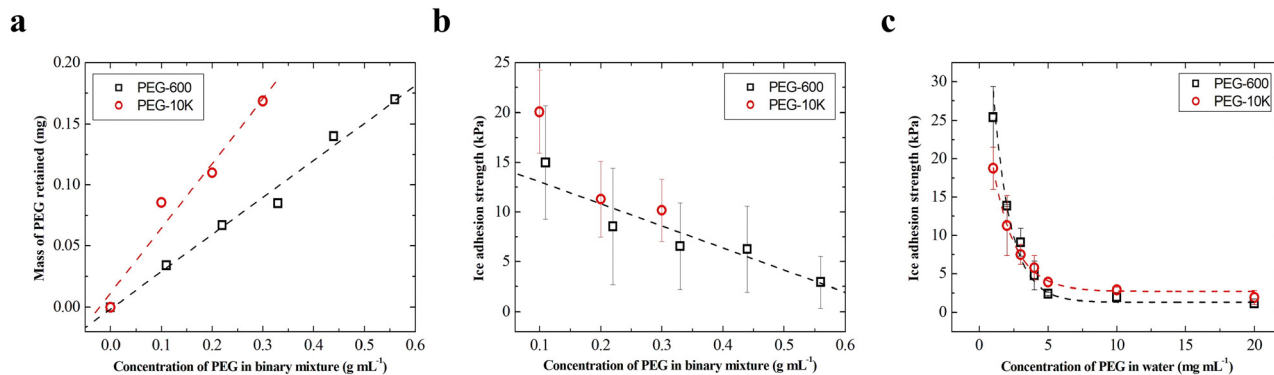


Fig. 3 (a) Mass of PEG retained in 1 mg of MSP/SBS composite (30% by mass MSP) as a function of PEG concentration in the binary solvent mixture. (b) Ice adhesion strength on PEG filled composites of (a) at $-10\text{ }^{\circ}\text{C}$. (c) Ice adhesion strength of PEG containing ice columns at $-10\text{ }^{\circ}\text{C}$ on unfilled (no PEG) MSP/SBS composites (30% by mass MSP) as a function of PEG concentration in the frozen aqueous solution. PEG-600 (squares) and PEG-10k (circles).

For PEG-10k, the concentration of the filling solution was kept between 0 and 0.3 g mL^{-1} to ensure dissolution. Similar to the results of MSP filled in PEG solutions (Fig. 1e), the amount of PEG retained in MSP/SBS composites increased with the concentration of PEG in the binary solvent mixture. This increase was linear for both PEG with a larger slope for PEG-10k.

Anti-icing efficacy of the composite coatings was characterized by measuring the ice adhesion strength on MSP/SBS composites with an apparatus that contains a force probe and a sample holder placed in a cooling chamber (Fig. S1, ESI[†]). Despite the differences in the amount of PEG retained, composites filled with different molar mass PEG exhibited similar ice adhesion strength at $-10\text{ }^{\circ}\text{C}$, as shown in Fig. 3b. When PEG-600 or PEG-10k was filled into MSP/SBS composites, the ice adhesion strength decreased with increasing amount of retained PEG in the composite (increasing concentration of PEG filling solution) from 15–20 kPa at 10 volume% PEG concentration to $3 \pm 2\text{ kPa}$ for the composites filled in 50 vol% PEG solutions. The decrease in ice adhesion strength on filled composites can be attributed to the formation of a lubricating liquid layer of PEG and water between the ice and the composite induced by PEG present and/or released at the surface.^{31,40} Such a lubricating layer, depending on its thickness, can also minimize the mechanical interlocking between the ice and the composite due to surface roughness. With increasing amount of retained PEG in the composite, more PEG is released at the ice/composite interface and forms a thicker lubricating liquid layer of PEG/water resulting in lower ice adhesion strength.

To ensure the presence of PEG molecules at the ice/composite interface in a model experiment and to check the effectiveness of different molar mass PEG chains in anti-icing, PEG-600 or PEG-10k containing aqueous solutions were frozen on unfilled MSP/SBS composites and the ice adhesion strength was measured at $-10\text{ }^{\circ}\text{C}$. PEG concentration in the frozen aqueous solution was varied between 1 and 20 mg mL^{-1} . Fig. 3c shows the ice adhesion strength of PEG-containing ice columns on unfilled composites as a function of PEG concentration in the frozen

aqueous solution. No significant difference in ice adhesion strength was observed between PEG-600 and PEG-10k. The ice adhesion strength initially decreased fast from 20–25 kPa for 1 mg mL^{-1} PEG containing ice to 3–4 kPa for 5 mg mL^{-1} PEG containing ice. For PEG concentrations in ice above 5 mg mL^{-1} , the ice adhesion strength decreased rather slowly to 1–2 kPa at 20 mg mL^{-1} PEG in ice. These ice adhesion values are similar to that between ice (formed by DI water) and the MSP/SBS composite filled in 50 vol% PEG solution (Fig. 3b). The results in Fig. 3c indicate a lower bound in ice adhesion strength at $-10\text{ }^{\circ}\text{C}$ for interfacial PEG density corresponding to that of the cross-section of 5 mg mL^{-1} aqueous PEG solution. These results clearly imply that the observed extremely low ice adhesion strength in the case of filled MSP/SBS composites is due to the presence of PEG at the ice/composite interface which forms a lubricating liquid layer of PEG/water and decreases the ice adhesion strength down to extremely low values of 1–5 kPa. Because lower molar mass PEG-600 (fluid at room temperature) retained in the composite showed linear dependence in a larger PEG concentration range of 10–50% by volume ($0.11\text{--}0.56\text{ g mL}^{-1}$), PEG-600 filled composites were used in further characterization.

Surface wettability and freezing delay of anti-icing composites

Surface wettability and anti-icing functionality of PEG-filled MSP/SBS composite coatings were investigated by measuring the water contact angles and freezing time of water droplets placed on the composite surfaces, respectively, at different temperatures. Fig. 4a shows the water contact angles as a function of the measurement temperature which was varied between $25\text{ }^{\circ}\text{C}$ and $-10\text{ }^{\circ}\text{C}$. Water contact angles on bare glass slides, SBS coating and unfilled MSP/SBS composites were used as controls. Water contact angles decreased with decreasing temperature on all samples. This temperature-dependent decrease in contact angles is attributed to the condensation of water vapor on the samples. While the hydrophilic bare glass surfaces exhibited the lowest water contact angles decreasing from 55° at $25\text{ }^{\circ}\text{C}$ to 35° at $-10\text{ }^{\circ}\text{C}$, the water contact angles on the hydrophobic SBS films were the highest changing between 110° and 55° in the temperature range of $25\text{ }^{\circ}\text{C}$ and $-10\text{ }^{\circ}\text{C}$,



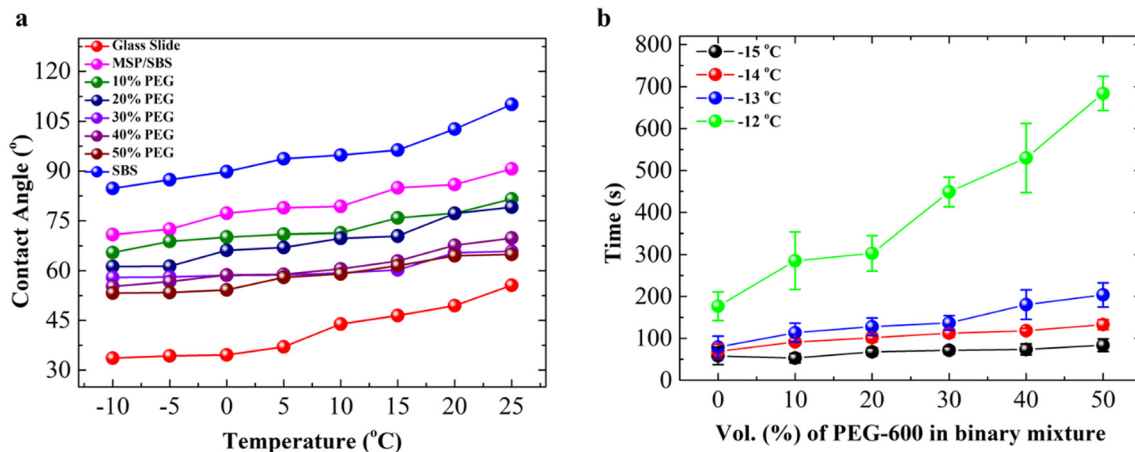


Fig. 4 Surface wettability and anti-icing performance of MSP/SBS composites. (a) Water contact angles on the MSP/SBS composites as a function of plate temperature. The standard deviations of the measured contact angles were between 0.5 and 1.5°. (b) Freezing time of water droplets on MSP/SBS composite coatings as a function of PEG-600 concentration of the filling solution.

respectively. The loading of hydrophilic MSP (30% by weight) in the SBS matrix decreased the contact angles by 15°–20° as compared to SBS samples. The surface roughness due to the addition of MSP in the SBS matrix is also expected to contribute to enhanced wetting and lower contact angles on unfilled MSP/SBS composite surfaces. Water contact angles decreased further with the incorporation of hydrophilic PEG-600 into the pores of MSP in the composites. The contact angles on PEG-600 filled MSP/SBS coatings changed between 78° and 52° in the temperature range of the measurements. The contact angle for PEG-600 filled MSP/SBS composites decreased with increasing concentration of PEG filling solution in the binary mixture, in other words with the PEG amount retained in the composites (Fig. 3a).

PEG-filled composites also showed weaker temperature dependence compared to the control samples. The temperature-dependent decrease in contact angle values was 10°–15° for PEG filled samples as compared to 20°–25° for SBS and MSP/SBS composites. The weaker temperature dependence is due to the presence of hydrophilic PEG-600 on the surface of the composites facilitating the adsorption of water vapor even at room temperature. Despite the solubility of PEG-600 in water, the measured water contact angles were in the range of 75°–52° for the PEG-filled MSP/SBS composites. This can be attributed to the presence of islands of PEG-600 filled surface-exposed pores of MSP on the composite coatings. The decrease in water contact angles on PEG-filled MSP/SBS composites confirms the presence of hydrophilic PEG-600 in MSP at the top surface and the possible release of PEG upon contact with water. The presence and release of PEG-600 also contribute to the reduction of the freezing time and ice adhesion strength as presented below.

The anti-icing functionality of PEG-filled MSP/SBS composites was evaluated by comparing the freezing time of 5 μ L water droplets on the surface of the coatings at a constant temperature. Fig. 4b shows the variation of the freezing time of water droplets on the MSP/SBS composite surfaces at different temperatures as a function of PEG-600 concentration of the

filling solution which is proportional to the amount of PEG retained in the composite (Fig. 3a). The freezing time on unfilled MSP/SBS composites increased from 58 s at –15 °C to 177 s at –12 °C indicating the fact that ice nucleation probability decreases with increasing temperature. On unfilled MSP/SBS composites, the unfavorable interaction between water and hydrophobic composite surfaces along with the larger contact angles contributes to the freezing delay. As the amount of PEG retained in the composite increased with increasing PEG concentration of the filling solution, the freezing time on PEG-filled MSP/SBS composites increased at constant temperature.

The freezing time of water droplets at –12 °C increased from 170 s for unfilled MSP/SBS composites to 290 s for MSP/SBS composites filled in 10 vol% PEG-600 solutions and gradually increased to 684 s for the composites filled in 50 vol% PEG-600 solutions. The increase in freezing delay of water droplets on MSP/SBS composites filled in PEG solutions of different concentrations (10–50 vol%) can be attributed to the presence/release of PEG-600 at the water/composite interface. The release of hydrophilic PEG-600 into the water droplets placed on the MSP/SBS composite surfaces decreases its freezing temperature and delays the freezing process at the specific temperature. The release of PEG-600 into water droplets is expected to originate mainly from the surface exposed pores of MSP in MSP/SBS composites considering the inability of water to swell SBS and that loosely bound PEG on the MSP/SBS composite surface was removed by rinsing prior to freezing experiments.

Ice adhesion and accumulation on anti-icing composites

Ice adhesion strength on bare glass substrates was measured as control experiments in the temperature range of –10 °C to –20 °C and was found to decrease from 420 \pm 42 kPa to 341 \pm 26 kPa as the measurement temperature increased from –20 °C to –10 °C (Fig. S5a, ESI†). The values on bare glass and the decreasing trend with increasing temperature are consistent with the previously reported values of ice adhesion strength



which are in the range of 366 ± 23 kPa.^{32,41} When SBS is coated on glass substrates, the ice adhesion strength decreased to 50 ± 10 kPa at -10 °C (Fig. S5b, ESI†). This reduction in ice adhesion strength on SBS coated surfaces can be caused by the hydrophobicity of SBS and its smoother surface texture which can reduce any possible mechanical interlocking.

As shown in Fig. 5a, the introduction of hydrophilic MSP into SBS increased the ice adhesion strength to 173 ± 40 kPa at -10 °C compared to that on the SBS surface due to increased surface hydrophilicity (Fig. 4a) and surface roughness which resulted in stronger adhesion and mechanical interlocking between ice and the composite surface. When PEG-600 was filled into MSP/SBS composites, the ice adhesion strength was decreased significantly by an order of magnitude to 15 ± 5 kPa for the composites filled in 10 vol% PEG solutions. With increasing amount of retained PEG in the composite (increasing concentration of PEG-600 filling solution), ice adhesion strength on filled MSP/SBS gradually decreased to 3 ± 2 kPa for the composites filled in 50 vol% PEG solutions.

To show that the release of PEG is a critical factor in the measured ice adhesion strength, ice adhesion measurement was done on an MSP/SBS composite filled in 50 vol% PEG solution after keeping the composite in water for different time intervals. Fig. 5b shows the ice adhesion strength at -10 °C on the filled composite as a function of immersion time in water. The results showed that the ice adhesion strength on the composite gradually increased from 3 kPa right after filling to 153 kPa for the composite kept in water for 20 min. Considering that the ice adhesion strength on the unfilled MSP/SBS composite was 173 kPa (Fig. 5a), it can be concluded that almost all of the PEG from the surface exposed MSP is released when kept in water and the remaining PEG is not enough to form a lubricating liquid layer of PEG/water at the ice/composite interface to significantly lower ice adhesion. Because water can't swell SBS, PEG retained in pores deeper below the surface is expected to be trapped and can only be effective in case of wear and/or scratches at the top surface exposing them to the water/composite interface.

The longevity of the icephobic properties in terms of ice adhesion strength of filled MSP/SBS composite coatings was

demonstrated through consecutive icing/de-icing cycles. Fig. 5c shows the ice adhesion strength at -10 °C as a function of 15 consecutive measurements on MSP/SBS composites filled in 50 vol% PEG solution in the binary mixture. The ice adhesion strength increased in consecutive measurements faster for the first 4 icing/deicing cycles (from 1.5 kPa to 4 kPa at the 4th cycle) and then rather slowly beyond that (from 4 kPa to 5 kPa at the 15th cycle). This indicates a rather slow release (and removal with ice) of PEG at -10 °C from surface-exposed pores of MSP. The observation that the ice adhesion strength is very low (~ 5 kPa) even at the 15th icing/de-icing cycle clearly shows that the filled MSP/SBS coatings can have a long lifetime at sub-zero temperatures.

The accumulation of frost induced by spraying water droplets at 0 °C onto inclined (by 45°) PEG-filled MSP/SBS composites at -10 °C was investigated as a measure of anti-frosting functionality. The amount of frost accumulated on the surfaces was gravimetrically determined. Fig. S6 in the ESI† shows the mass of accumulated frost on the surface as a function of PEG-600 concentration in the binary solvent in which the composites were filled. Bare glass substrates and unfilled MSP/SBS composites were measured as control samples. The amount of frost accumulated on glass slides after spraying was measured to be 20.0 mg cm⁻² which decreased to 17.0 mg cm⁻² on unfilled MSP/SBS composites. The decrease in frost accumulation on unfilled MSP/SBS composites can be attributed to the easier removal of the landing and/or accumulated water/ice droplets due to the higher water contact angles of the composites as compared to glass slides (Fig. 4a). For MSP/SBS composites filled with PEG-600, the frost accumulation decreased further to 14.5 ± 1.5 mg cm⁻² independent of the PEG concentration of the filling solutions. Considering that PEG is located in the pores of MSP and the surface density of MSP is expected to be constant for all composites (30% by weight MSP in the composites), it is understandable that the accumulated frost does not show any dependence on the PEG retained. The results showed that the accumulation of frost on PEG-600 filled films is ~ 25 –30% lower than that on glass slides and ~ 15 % lower than that on unfilled MSP/SBS composites. It is expected that PEG-600 prevents the freezing of the landing/accumulated

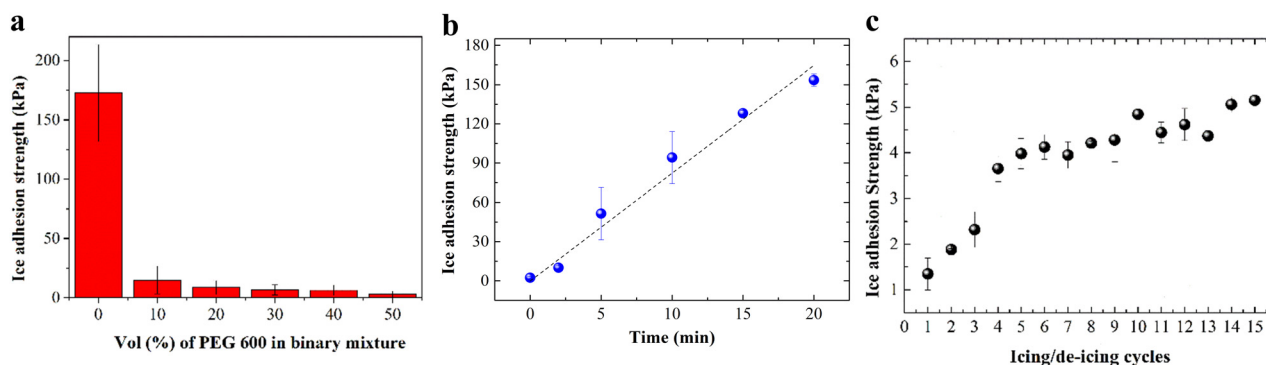


Fig. 5 Ice adhesion strength measurements of MSP/SBS composites at -10 °C: (a) ice adhesion strength as a function of PEG-600 concentration in the filling solution, (b) ice adhesion strength of composite coatings filled in 50 vol% PEG solutions as a function of dipping time in DI water, (c) ice adhesion strength as a function of the icing/de-icing cycle on MSP/SBS composites filled in 50 vol% PEG solution in the binary mixture.



water droplets which can then easily slide down the inclined surface of the filled MSP/SBS composite.

The anti-icing characterization and ice adhesion measurements of PEG-filled MSP/SBS composites showed that the release of PEG from the surface exposed pores of MSP into the water placed on the surfaces is responsible for their superior anti-icing ability and low ice adhesion strength. The post filling of composite coatings with PEG implies that these composites can maintain anti-icing properties in the presence of surface scratches and wear due to the presence of PEG-filled pores of MSP buried in the SBS matrix. These results clearly demonstrate the potential of composites for longer-term use under harsh conditions.

Conclusions

Release-based extremely low ice adhesion strength and durable anti-icing coatings were designed and realized by loading MSP into the SBS matrix and filling PEG as the anti-icing agent into MSP/SBS composites. The coatings showed ice adhesion strength as low as 3 kPa. The mechanism for the low ice adhesion values was shown to be the presence of PEG at the ice/composite interface which is known to form a lubricating liquid layer of PEG/water at sub-zero temperatures. Frozen PEG-containing aqueous solutions on unfilled MSP/SBS composites showed a decrease in the ice adhesion strength with the PEG concentration in the aqueous solution to a constant value of 3 ± 1 kPa. The use of MSP with a SSA of $428 \text{ m}^2 \text{ g}^{-1}$ as the anti-icing agent carrier enhanced the amount of PEG retained in the composites by up to a factor of 2 compared to mainly macroporous DE having a SSA of $65 \text{ m}^2 \text{ g}^{-1}$. The freezing time of water droplets on the composites increased and the ice adhesion strength decreased with the amount of PEG retained in the composites. After 15 icing/deicing cycles, the ice adhesion strength was measured to be ~ 5 kPa indicating a rather slow release (and removal with ice) of PEG at -10°C from surface-exposed pores of MSP. Although the release of retained PEG from filled MSP/SBS composites in time increases the ice adhesion strength, the composites have the advantage of continuing anti-icing functionality upon possible wear and scratches in time due to surface exposure of filled MSP previously buried in the SBS matrix. These results clearly show that PEG filled MSP/SBS composites demonstrate a passive anti-icing mechanism based on sustained release of PEG with extremely low ice adhesion strength and significant potential for longer-term use in sub-zero temperature and harsh environments.

Author contributions

A. Ijaz (investigation; writing – original draft); A. Miko (conceptualization; investigation; writing – review & editing); A. L. Demirel (conceptualization; funding acquisition; supervision; writing – review & editing).

Conflicts of interest

There are no conflicts to declare.

Acknowledgements

The authors thank Turkish Scientific and Technological Research Council (TÜBİTAK, Project number 217M545) for funding, Dr Barış Yağcı for his support in SEM investigations, and Koç University Surface Science and Technology Center (KUYTAM) and Koç University Tüpraş Energy Center for the use of material characterization facility.

Notes and references

- 1 F. Lamraoui, G. Fortin, R. Benoit, J. Perron and C. Masson, *Atmos. Res.*, 2013, **128**, 57.
- 2 X. Huang, N. Tepylo, V. Pommier-Budinger, M. Budinger, E. Bonaccorso, P. Villedieu and L. Bennani, *Prog. Aerosp. Sci.*, 2019, **105**, 74.
- 3 T. M. Schutzius, S. Jung, T. Maitra, P. Eberle, C. Antonini, C. Stamatopoulos and D. Poulidakos, *Langmuir*, 2015, **31**, 4807.
- 4 W. Li, Y. Zhan and S. Yu, *Prog. Org. Coat.*, 2021, **152**, 106117.
- 5 A. Azimi Yancheshme, G. Momen and R. Jafari Aminabadi, *Adv. Colloid Interface Sci.*, 2020, **279**, 102155.
- 6 M. J. Kreder, J. Alvarenga, P. Kim and J. Aizenberg, *Nat. Rev. Mater.*, 2016, **1**, 15003.
- 7 H. Sojoudi, M. Wang, N. Boscher, G. H. McKinley and K. K. Gleason, *Soft Matter*, 2016, **12**, 1938.
- 8 Y. Hou and K. L. Choy, *Prog. Org. Coat.*, 2022, **163**, 106637.
- 9 Z. Chu, W. Jiao, Y. Huang, M. Yan, Y. Zheng, R. Wang and X. He, *Adv. Mater. Interfaces*, 2020, **7**, 2000492.
- 10 A. J. Meuler, J. D. Smith, K. K. Varanasi, J. M. Mabry, G. H. McKinley and R. E. Cohen, *ACS Appl. Mater. Interfaces*, 2010, **2**, 3100.
- 11 L. Cao, A. K. Jones, V. K. Sikka, J. Wu and D. Gao, *Langmuir*, 2009, **25**, 12444.
- 12 C. H. Moon, S. Yasmeen, K. Park, H. Gaiji, C. Chung, H. Kim, H.-S. Moon, J. W. Choi and H.-B.-R. Lee, *ACS Appl. Mater. Interfaces*, 2022, **14**, 3334.
- 13 Y. Lin, H. Chen, G. Wang and A. Liu, *Coatings*, 2018, **8**, 208.
- 14 L. B. Boinovich and A. M. Emelyanenko, *Mendeleev Commun.*, 2013, **23**, 3.
- 15 H. Niemelä-Anttonen, H. Koivuluoto, M. Tuominen, H. Teisala, P. Juuti, J. Haapanen, J. Harra, C. Stenroos, J. Lahti and J. Kuusipalo, *Adv. Mater. Interfaces*, 2018, **5**, 1800828.
- 16 K. Golovin, S. P. Kobaku, D. H. Lee, E. T. DiLoreto, J. M. Mabry and A. Tuteja, *Sci. Adv.*, 2016, **2**, e1501496.
- 17 K. Golovin and A. Tuteja, *Sci. Adv.*, 2017, **3**, e1701617.
- 18 A. Ijaz, A. Miko and A. L. Demirel, *New J. Chem.*, 2018, **42**, 8544.
- 19 S. F. Wen, Y. M. Wang, Z. M. Zhang and Y. L. Liu, *Prog. Org. Coat.*, 2019, **137**, 105320.
- 20 Y. Han Yeong, A. Steele, E. Loth, I. Bayer, G. De Combarieu and C. Lakeman, *Appl. Phys. Lett.*, 2012, **100**, 053112.
- 21 T. Verho, C. Bower, P. Andrew, S. Franssila, O. Ikkala and R. H. Ras, *Adv. Mater.*, 2011, **23**, 673.



- 22 L. B. Boinovich, A. M. Emelyanenko, K. A. Emelyanenko and E. B. Modin, *ACS Nano*, 2019, **13**, 4335.
- 23 T.-S. Wong, S. H. Kang, S. K. Y. Tang, E. J. Smythe, B. D. Hatton, A. Grinthal and J. Aizenberg, *Nature*, 2011, **477**, 443.
- 24 J. Sarma, L. Zhang, Z. Guo and X. Dai, *Chem. Eng. J.*, 2021, **431**, 133475.
- 25 C. J. Prakash and R. Prasanth, *Surf. Interfaces*, 2020, **21**, 100678.
- 26 C. Liu, Y. Li, C. Lu, Y. Liu, S. Feng and Y. Liu, *ACS Appl. Mater. Interfaces*, 2020, **12**, 25471.
- 27 Y. Long, X. Yin, P. Mu, Q. Wang, J. Hu and J. Li, *Chem. Eng. J.*, 2020, **401**, 126137.
- 28 S. Ozbay, C. Yuceel and H. Y. Erbil, *ACS Appl. Mater. Interfaces*, 2015, **7**, 22067.
- 29 Z. He, Y. Zhuo, F. Wang, J. He and Z. Zhang, *Prog. Org. Coat.*, 2020, **147**, 105737.
- 30 J. Chen, R. Dou, D. Cui, Q. Zhang, Y. Zhang, F. Xu, X. Zhou, J. Wang, Y. Song and L. Jiang, *ACS Appl. Mater. Interfaces*, 2013, **5**, 4026.
- 31 D. Chen, M. D. Gelenter, M. Hong, R. E. Cohen and G. H. McKinley, *ACS Appl. Mater. Interfaces*, 2017, **9**, 4202.
- 32 S. Chernyy, M. Järn, K. Shimizu, A. Swerin, S. U. Pedersen, K. Daasbjerg, L. Makkonen, P. Claesson and J. Iruthayaraj, *ACS Appl. Mater. Interfaces*, 2014, **6**, 6487.
- 33 R. Dou, J. Chen, Y. Zhang, X. Wang, D. Cui, Y. Song, L. Jiang and J. Wang, *ACS Appl. Mater. Interfaces*, 2014, **6**, 6998.
- 34 S. Kanyas, D. Aydın, R. Kizilel, A. L. Demirel and S. Kizilel, *PLoS One*, 2014, **9**, e88125.
- 35 D. Aydın, R. Kizilel, R. O. Caniaz and S. Kizilel, *Ind. Eng. Chem. Res.*, 2015, **54**, 12587.
- 36 J. Ayres, W. Simendinger and C. Balik, *J. Coat. Technol. Res.*, 2007, **4**, 473.
- 37 X. Sun, V. G. Damle, S. Liu and K. Rykaczewski, *Adv. Mater. Interfaces*, 2015, **2**, 1400479.
- 38 A. Ijaz, G. Topcu, M. H. Qureshi, A. Miko and A. L. Demirel, *Colloids Surf., A*, 2021, **615**, 126203.
- 39 T. Inada, T. Koyama, F. Goto and T. Seto, *J. Phys. Chem. B*, 2012, **116**, 5364.
- 40 B. Zobrist, U. Weers and T. Koop, *J. Chem. Phys.*, 2003, **118**, 10254.
- 41 T. Yamazaki, M. Tenjimabayashi, K. Manabe, T. Moriya, H. Nakamura, T. Nakamura, T. Matsubayashi, Y. Tsuge and S. Shiratori, *Ind. Eng. Chem. Res.*, 2019, **58**, 2225.
- 42 C. Chircov, A. Spoială, C. Păun, L. Crăciun, D. Ficăi, A. Ficăi, E. Andronescu and Ş. C. Turculeţ, *Molecules*, 2020, **25**, 3814.
- 43 A. Ijaz, M. B. Yagci, C. W. Ow-Yang, A. L. Demirel and A. Mikó, *Microporous Mesoporous Mater.*, 2020, **303**, 110240.
- 44 Z. Jia and C. Tian, *Desalination*, 2009, **247**, 423.

